Effect of the neodymium doping on the magnetic and structural properties of the Sr-hexaferrite obtained by the Pechini method

M.F. Ramírez-Ayala, T.J Pérez-Juache, A.M. Herrera-González, A. Lobo Guerrero

In this work, neodymium (Nd^{3+}) doped strontium hexaferrite was obtained using the sol–gel based Pechini method. The cation distribution was modified by doping with different amounts of Nd^{3+} ions when $0.0 \leq x \leq 0.4$ according to the chemical expression $Sr_{1-x}Nd_xFe_{12}O_{19}$ the powders were sintered at 1100 °C for 1 h. The influence of the neodymium was analyzed, and the magnetic and structural properties have been associated with the fabrication method. The crystalline phases, structure, and particle morphology of the samples were determined by X-ray diffraction, scanning electron microscopy, and transmission electron microscopy. In addition, the magnetic properties were measured at room temperature using a vibrating sample magnetometer with an applied field of up to 20 kOe. Moreover, magnetization and coercivity values are influenced by the neodymium content. The results showed that the Pechini sol-gel method allows a limited solubility of the Nd^{3+} ions on the hexaferrite structure.

Introduction

Recently, M-type hexagonal ferrites have attracted considerable attention due to their potential and technological applications. These materials were discovered in the 1950s when they were first magnetically characterized by Phillips labs [1]. They have been used as permanent magnets due to their rather good energy product and the excellent cost-performance ratio [2]. There are even reports on the use of these materials in the area of photocatalysis because they can be magnetically extracted after each treatment and furthermore are active in the visible spectrum.

In addition, M-type strontium hexaferrite is considered a synthetic magnetic material of great interest due to its characteristics such as excellent chemical stability, high Curie temperature, and corrosion resistance. Moreover, it presents outstanding magnetic properties like high saturation magnetization, high coercivity, and high uniaxial magnetocrystalline anisotropy [3,4].

This compound has a hexagonal packing structure, in other words, a magnetoplumbite type crystal structure with chemical formula $MFe_{12}O_{19}$ (where M are divalent cations such as Sr^{2+}, Ca^{2+}, Ba^{2+} or Pb^{2+}), a space group $P6_3/mmc$ and 64 ions per unit cell [5]. The crystal structure and some of the physical properties of ferrites type M can be controlled by multiple manufacturing processes and the parameters associated with their sintering [6]. These properties strongly depend upon the precursors and synthesis method. For preparing these materials several physical and chemical synthesis methods have been reported, such as Pechini sol-gel [7], molten salts, high energy grinding [8], sonochemistry [9], hydrothermal [10], and pyrolysis [11]. The Pechini sol-gel method has great advantages over other methods to obtain materials with the desired shape and depending on the experimental parameters, obtain up to nanometric size. In this sense, multiple factors intervene in obtaining the final product, such as the relationship between the precursor salts, reaction of temperature, pH, and sintering time/temperature [12].

On the other hand, it has been reported that by doping with rare earth elements their thermal, electrical, magnetic, and optical properties can be improved, in addition to having some other applications [13]. Considering the above-mentioned issues, doping with the correct ratio of rare earth elements on strontium hexaferrite is important to improve even the structural and magnetic properties [14]. These improvements can be achieved by doping with rare earth trivalent cations, for example, Nd^{3+} [15-18], La^{3+} [19,20], Pr^{3+} [21,22], and Gd^{3+} [23]. These elements are the most studied and therefore have had the greatest impact on various investigations although there are more possibilities of rare earth for doping such as Sm^{3+}, Er^{3+}, Yb^{3+}, Eu^{3+}, and Dy^{3+} [24,25].

The study of these rare earth elements is so extensive that there are even reports of the use of these cations as substituents within the hexaferrite structure in combination with cobalt to increase the solubility of these rare earth. These substitutions primarily involve certain factors. For example, earth ions with a higher atomic radius have a substitution limit whereby it is difficult to enter lattice sites, consequently this leads to crystal collapse and distortion of the strontium hexaferrite lattice [26]. In this sense, it is of great importance for the previous study to carry out satisfactorily the substitution with these elements.

In this work, the synthesis was carried out by the Pechini sol-gel method and the characterization of strontium hexaferrite doped with Nd^{3+} with the purpose of studying the systematic contribution of the structural, microstructural and magnetic properties.

M.F. Ramírez-Ayala ✉ ⓘ, A.M. Herrera-González ⓘ,
A. Lobo Guerrero ✉ ⓘ
*Área Académica de Ciencias de la Tierra y Materiales,
Universidad Autónoma del Estado de Hidalgo,
Pachuca, Hgo., 42184, México.*

T.J. Pérez-Juache
*Unidad Morelia, Instituto de Investigaciones en Materiales,
Universidad Nacional Autónoma de México,
Morelia, Mich., 58190, México.*

Experimental details

The Pechini method consists of the preparation of a polymeric resin from organic acids, alcohols, and the ions required for the desired material. Both the acid and alcohol must be poly-functional compounds (contain two or more functional groups) for preparing a desirable three-dimensional polymeric network [3,27]. The precursors used were $Sr(NO_3)_2$ (99%, Sigma-Aldrich), $Fe(NO_3)_3 \cdot 9H_2O$ (99%, Sigma-Aldrich), $Nd(NO_3)_3 \cdot 6H_2O$ (99%, Sigma-Aldrich), citric acid monohydrate (99%, JT Baker) and ethylene glycol (99%, Sigma-Aldrich). The precursor salts of strontium, iron and neodymium were weighted to obtain 1.0 g of the hexaferrite and were mixed in stoichiometric ratios following the chemical equation (1):

$$(1-x)Sr(NO_3)_2 + 12Fe(NO_3)_3 \cdot 9H_2O + xNd(NO_3)_3 \cdot 6H_2O + C_6H_8O_7 \cdot H_2O + C_2H_6O_2 \rightarrow Sr_{1-x}Nd_xFe_{12}O_{19} + CO_2 \uparrow + NO_2 \uparrow \quad (1).$$
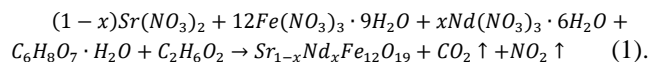
When x = 0.0, 0.1, 0.2, 0.3 and 0.4 labeled as SrM, SrM1, SrM2, SrM3, and SrM4, respectively. First, the nitrates were dissolved into deionized water under constant stirring. Then citric acid and ethylene glycol were added to the solution of nitrates. The nominal molar ratio of metal ions to citric acid within the mixture was kept constant at 1:5. The resultant solution was heated at 70 °C for dehydration, and later at 100 °C for polymerization (where intermediate reactions occur to obtain the polymer resin). The resins were then preheated at 370 °C for 45 minutes and crushed in an agate mortar. The crushed resins were calcined to 1100 °C for 1 h in air to obtain crystalline powders.

The crystal structure was confirmed by X-ray diffraction (XRD) measurements. The analysis by X-ray diffraction was performed using a D2 Phaser diffractometer (Bruker) with Cu Kα radiation (Kα$_1$ = 1.5406 Å, and Kα$_2$ = 1.5444 Å, with a Kα$_2$/Kα$_1$ ratio of 0.5) within a 2θ angular range from 20° to 80° operated at 30 KV and 10 mA. The microstructure and morphological characteristics of the calcined powders were observed by the SEM images, using a Scanning Electron Microscope (SEM) JEOL JSM-IT300, and TEM images using a Transmission Electron Microscope (TEM) JEOL JEM-ARM200F. Magnetic hysteresis loops (M-H) were obtained using a Quantum Design VSM magnetometer (Quantum Design, Inc., San Diego, CA, USA). The hysteresis curves were obtained with a magnetic field of 20 kOe at room temperature.

Results and discussion

Structural properties

The X-ray diffraction (XRD) patterns of the strontium hexaferrite doped with Nd^{3+} obtained at 1100 ℃ are shown in Figure 1. The diffractograms of all samples were analyzed using the Rietveld refinement method and the MAUD program [28] to obtain the structural parameters. The model used for the refinement procedure was based on the strontium hexaferrite (COD ID - 1006000), hexagonal symmetry with P6$_3$/mmc space group, and lattice parameters a = 5.8844 Å, c = 23.050 Å [29]. Figure 1 shows the experimental (I_{Obs}) and the refined (I_{Calc}) X-ray patterns for
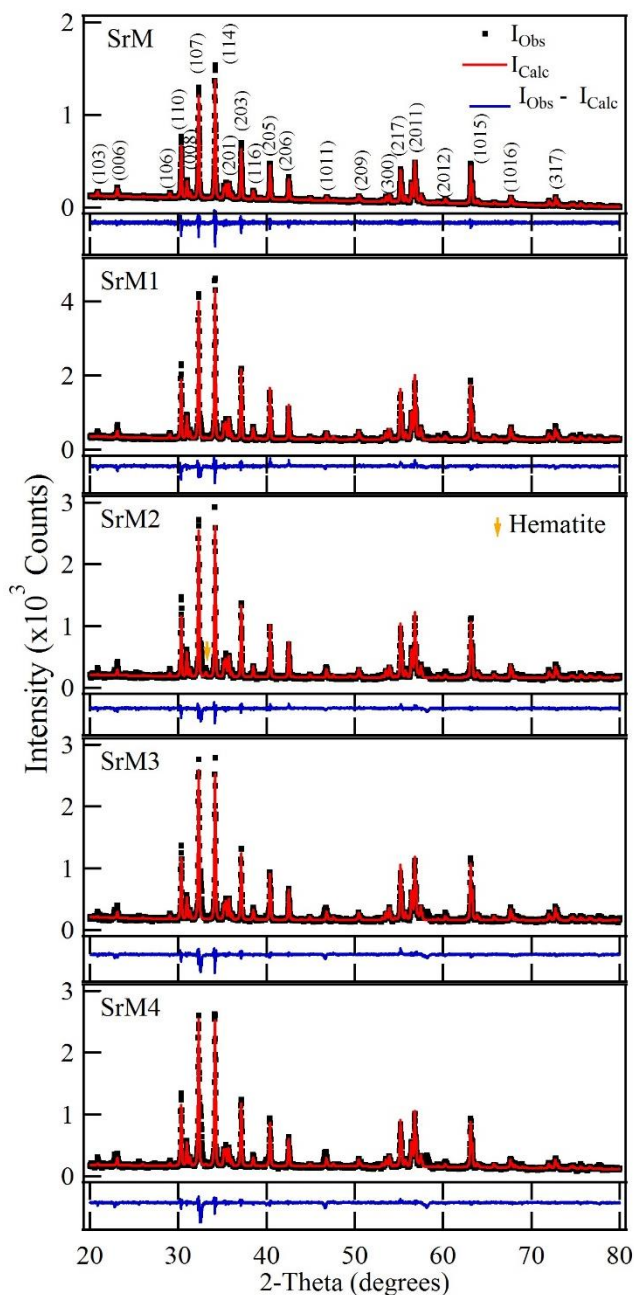
Figure 1. Powder XRD patterns of the hexaferrite doping with Nd^{3+} in different proportions.

the samples. The refinement final output R_{wp}, R_{exp}, and Chi-squared $\chi^2 = (R_{wp}/R_{exp})^2$ are shown in Table 1 with the refined lattice parameter, X-ray density, and unit cell volume. The Rietveld analysis showed an increase in the crystallite size as the amount of neodymium increased.

Iron oxide (α-Fe_2O_3) was detected as a minor secondary phase due to an incomplete reaction of the precursors [30]. The lattice parameters of all the prepared samples were compared in Table 1. The lattice constant a remained almost constant, while c varied slightly with the Nd^{3+} concentration. Thus, the behavior of the lattice parameters with the neodymium doping suggests the possibility that the Nd^{3+} entered into the hexaferrite structure [31].

Table 1. Rietveld refinement results as a function of the Nd^{3+} content.

Sample ID	Nd (x)	Lattice parameters (Å)			X-ray density ($g\ cm^{-3}$)	V_{cell} (Å^3)	Fe_2O_3 (wt%)	Rietveld parameters		
		a	c	c/a				R_{wp} (%)	R_{exp} (%)	χ^2
SrM	0.0	5.8844(1)	23.0611(3)	3.9190	5.098	691.54	0.0	2.79	2.12	1.316
SrM1	0.1	5.8841(4)	23.0702(4)	3.9208	5.093	691.74	0.0	8.69	5.25	1.655
SrM2	0.2	5.8844(1)	23.0681(5)	3.9202	5.097	691.75	2.20	12.13	6.73	1.461
SrM3	0.3	5.8853(1)	23.0705(5)	3.9200	5.095	692.01	0.99	13.34	6.78	1.505
SrM4	0.4	5.8851(1)	23.0733(5)	3.9206	5.094	692.07	0.36	15.59	7.15	1.311

The behavior of V_{cell} may be attributed to the presence of the rare earth element because it tends to form strong lanthanide-oxygen bonds [32]. The binding energy of the octahedral lanthanide-oxygen in oxide materials is believed to be considerably higher than that for octahedral ion-oxygen transition metal. This phenomenon may be the reason for the shrinkage or expansion of the crystal lattice [33].

The crystallite size has been found to increase by increasing the concentration of Nd^{3+} as a doping element. This might happen mainly due to two reasons: firstly, the strain produced in the unit cell [34], and secondly, the diffusion inhibition of rare-earth elements in hexagonal structure [35]. Figure 2 shows the relationship between the Nd^{3+} concentration and the lattice constants a and c, as well as the relationship between the Nd^{3+} concentration and the c/a lattice parameters ratio.

In the present study, we found that the lattice parameters varied when increasing the Nd^{3+} concentration, and the behavior of the *c/a* ratio is mainly due to the chemical composition, defects, strain, and suppression effect of neodymium in strontium hexaferrite [30]. In addition, it has been reported that incorporating Nd^{3+} in the hexaferrite as a dopant leads to a significant variation in X-ray density, as observed in Table 1. The X-ray density is intimately related to the molecular weight of the sample and varies inversely

with the volume of the unit cell. The variation observed for the X-ray density as the doping concentration changes can be explained by the corresponding change in the lattice parameters and larger molecular weight of Nd^{3+} doping [36].

Magnetic properties

The hysteresis loops of strontium hexaferrite doped with neodymium at different ratios are shown in Figure 3. The presence of Nd^{3+} ions in the hexaferrite can affect the magnetic properties significantly. Table 2 summarizes the magnetic parameters such as saturation magnetization (M_s), remnant magnetization (M_r), squareness ratio M_r/M_s, and the coercive field (H_c). The obtained results show that the Nd^{3+} concentration mainly influences the magnetic properties. In general, as the Nd^{3+} concentration increases, M_s decreases while H_c increases, as shown in Figure 4.

Each Fe^{3+} ions possess 5 Bohr magnetons (μ_b) and the total magnetic moment per chemical formula unit in the M-type hexaferrite possesses is 20 μ_b [14]. This indicates that the magnetic moment of all the Fe^{3+} ions include seven Fe^{3+} ions, with two of them located each at 12k (↑) and $4f_2$ (↓) sublattices belonging to octahedral sites, one Fe^{3+} ion with the position at the 2b (↑) sublattice belonging to trigonal bipyramidal sites, and the last two at $4f_1$ (↓) sublattices belonging to tetrahedral sites. The arrows show the direction of the magnetic moment of the corresponding Fe^{3+} ions [37]. So, the saturation magnetization M_s, which is defined as the magnetic moment per unit mass of material, and remanence magnetization decrease as the Nd^{3+} concentration increases. The presence of impurities phases in the pure compound may
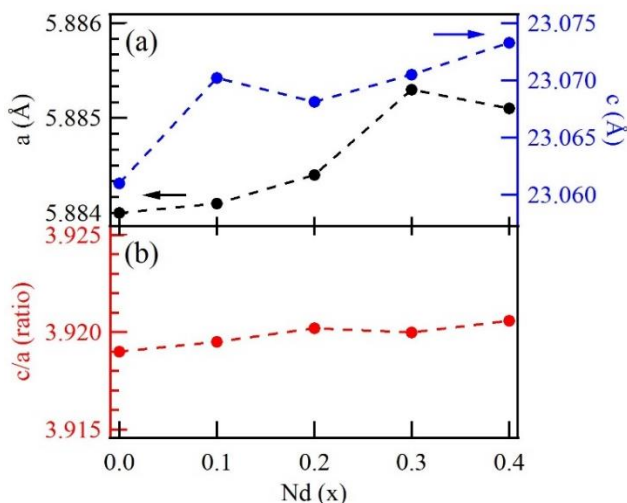
Figure 2. a) Lattice parameters *a* and *c*; b) c/a ratio as a function of the neodymium doping in the strontium hexaferrite.
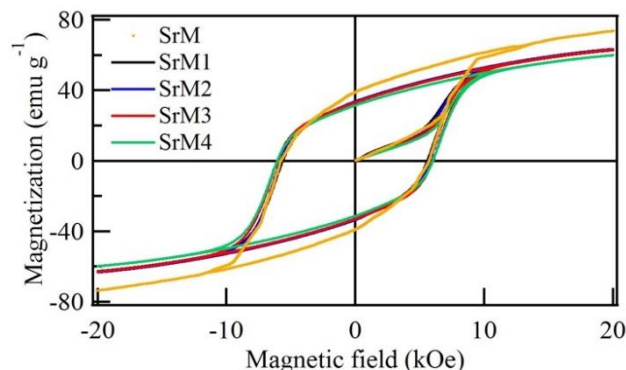
Figure 3. Major hysteresis loop of strontium hexaferrite and the doped hexaferrite with different amounts of neodymium.
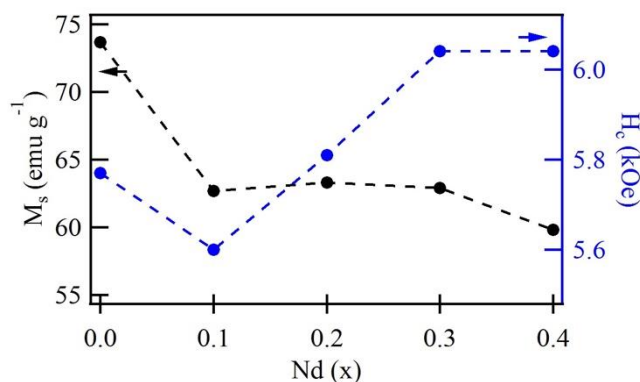
Figure 4. Saturation magnetization value (M_s) and coercivity field (H_c) of the samples doped Nd^{3+} at different ratios.

contribute to reducing the M_s value [38]. However, the coercivity (H_c) is related to the particle size. The increase in coercivity can be understood in terms of the increase in the anisotropy field because coercivity is proportional to the anisotropy constant according to the following relation [39]:

$$H_c = 2K/\mu_0 M_s \qquad (2)$$

Where K is the magnetocrystalline anisotropy and μ_0 the permittivity of free space ($4\pi \times 10^{-7}$ H m^{-1}), the observed increase of coercivity in accordance with the increase of neodymium concentration (up to x = 0.4) may be related to the increase in the magnetocrystalline anisotropy (K) and the grain size [40]. Also, it has been reported that the coercivity is proportional to the grain size. Besides, the increase in crystallite size with the decrease in density of Nd^{3+} leads to impeding the rotation of magnetization because the grain boundaries act as pinning centers [38].

The squareness ratio (M_r/M_s) of all samples doped is shown in Table 2. A squareness ratio (M_r/M_s) of 0.5 or above indicates a single magnetic domain on the material; in contrast, a ratio below 0.5 is attributed to a multidomain structure [41,42]. As can be seen in Table 2, the measured M_r/M_s ratio is approximately 0.53, indicating that the Nd^{3+} doped samples could exhibit a monodomain configuration [5]. In Figure 4, the relationship between saturation magnetization and coercivity is shown as well as the influence of neodymium as a doping element. Noting the decrease in M_s and increase in H_c. These results show that the magnetic properties are highly related to the synthesis conditions, such as temperature, neodymium concentration, and crystal size.

**Table 2**. Magnetic parameters of the Nd^{3+} doped strontium hexaferrite.

x	M_s (emu g^{-1})	M_r (emu g^{-1})	M_r/M_s	H_c (kOe)
0.0	73.69	39.18	0.5317	5.77
0.1	62.70	32.90	0.5247	5.60
0.2	63.30	33.56	0.5302	5.81
0.3	62.91	33.03	0.5251	6.04
0.4	59.83	31.40	0.5248	6.04
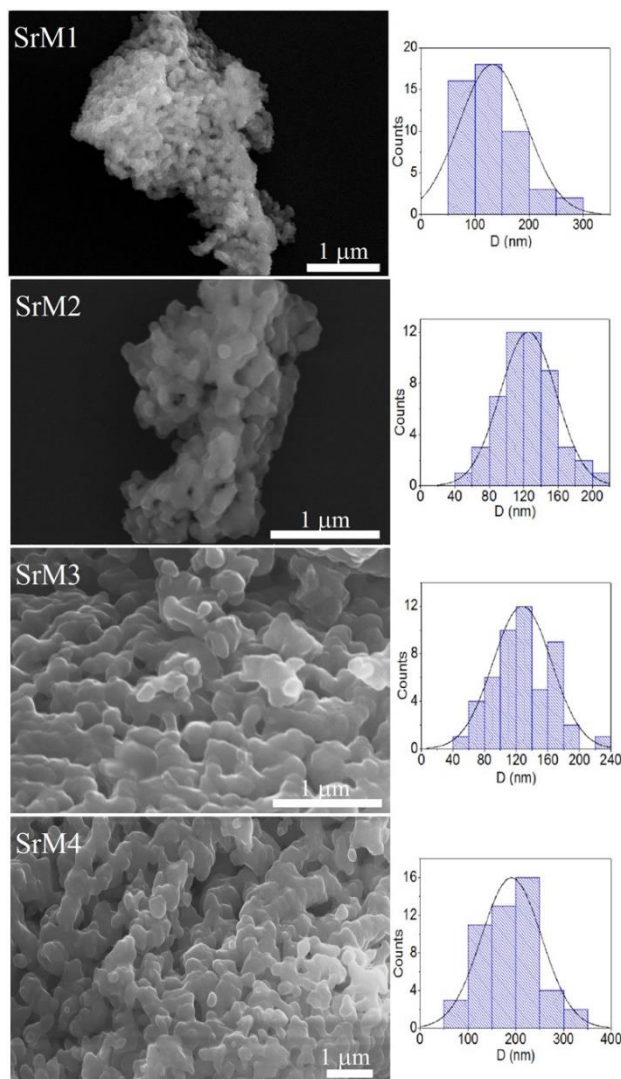
Figure 5. SEM micrographs of the strontium hexaferrite doped with different amounts of neodymium.

Morphological characteristics

Figure 5 shows the SEM micrographs and the particle size distributions of the strontium hexaferrite and the samples doped with different amounts of Nd^{3+}. In the sample SrM1, there are large crystal agglomerates of ~3.603 µm. The particles are semispherical and closely packed throughout the surface of the sample. The microstructures reveal that the neodymium content strongly influences the morphologies of prepared samples. As gradually increasing the Nd^{3+} concentration, the semispherical particles (SrM1) agglomerate and take on an elongated pattern, as shown for the samples SrM2, SrM3, and SrM4. It can also be seen that with the addition of Nd^{3+} content, agglomeration starts appearing, and particle size increases. The addition of Nd^{3+} into the hexaferrite also results in the aggregation of particles for higher compositions due to magnetic interactions between the neighboring particles [38]. The average particle size has been found to be 132, 125, 127, and 190 nm for SrM1, SrM2, SrM3, and SrM4, respectively.
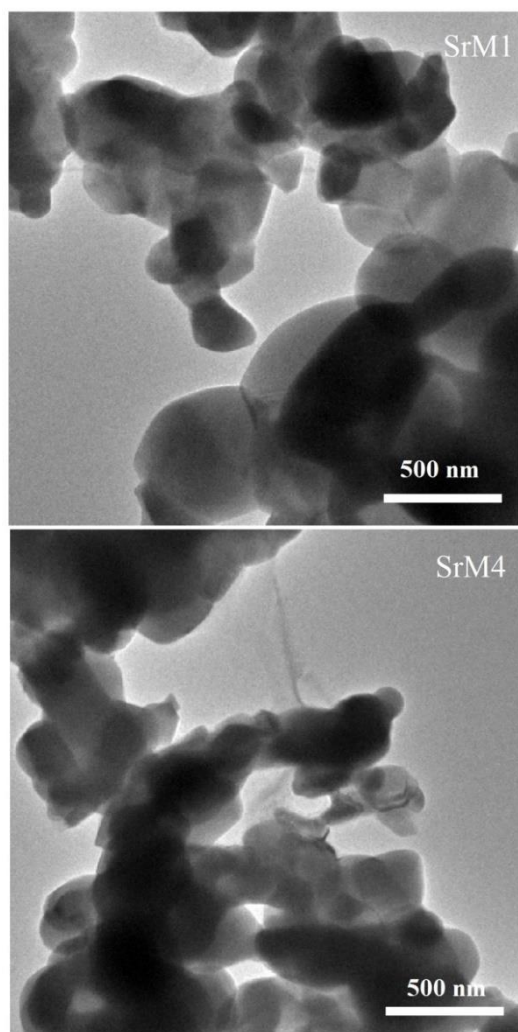
Figure 6. TEM micrographs for Strontium hexaferrite doped with different amounts of Nd^{3+}.

Figure 6 shows the TEM micrographs of the Nd-doped strontium hexaferrite with low and high ratios sintered at 1100°C for 1 h. As the doping amount increases, a higher degree of agglomeration is observed. That is, the increase in the proportion of Nd^{3+} facilitates particle growth. Also, spherical and semispherical shapes can be observed. The balance between nucleation and growth rate, which determines final particle size and morphology, depends on preparation conditions [43]. It has even been reported that in some cases, there is a preferential stacking (arrangement) in hexagonal-shaped particles. Therefore, the crystals tend to grow perpendicular to the c-axis, which makes the easy stacking of the platelet-like particles [44]. This effect is most likely due to the magnetic interactions between platelets [45].

Conclusions

The neodymium-doped strontium hexaferrite has been synthesized successfully using the Pechini sol-gel method. The close relationship between the crystal structure and the magnetic properties in the presence of Nd^{3+} was shown, as well as the influence caused by these cations on the structural parameters and the magnetic behavior of the hexaferrite. The Nd^{3+} doping caused marked variations in the lattice parameters, suggesting the Nd^{3+} enters the hexaferrite structure in a limited concentration which depends on the method and fabrication conditions. On the other hand, neodymium promotes changes at the structural and microstructural levels, which in turn modifies the coercive field as well as the expected values of the remanent and saturation magnetizations. In this sense, the strontium hexaferrite doped with neodymium could have a great impact on several technological applications due to its large capacity to induce intrinsic and extrinsic changes mainly due to an electronic reconfiguration and because the structural changes impact the functional properties.

References
[1]. R.C. Pullar, *Prog. Mater. Sci.* **57**, 1191 (2012).
[2]. W. Onreabroy, K. Papato, G. Rujijanagul, K. Pengpat, T. Tunkasiri, *Ceram. Int.* **38**, 415 (2012).
[3]. L. Klein, M. Aparicio, A. Jitianu, *Handbook of sol-gel science and technology: Processing, characterization and applications,* 2nd Ed. (Springer, 2018).
[4]. S. Rana, A. Gallo, R. Srivastava, R. Misra, *Acta Biomater.* **3**, 233 (2007).
[5]. M.A. Urbano, S.A. Palomares, I. Betancourt, T.J. Pérez, F. Ruiz, *Appl Phys. A* **125**, 1 (2019).
[6]. J.R. Lui, R.R. Hong, W.G. Feng, D. Badami, Y.Q. Wang, *Powder Technol.* **262**, 142 (2014).
[7]. S.M. Masoudpanah, A. Seyyed, *J. Magn. Magn. Mater.* **342**, 128 (2013).
[8]. K. Kim, K. Jeon, K.W. Moon, M.K. Kang, J. Kim, *IEEE Trans. Magn.* **52**, 1 (2016).
[9]. R.L. Palomino, A.M. Bolarín, F.N. Tenorio, F. Sánchez, C.A. Cortés, S. Ammar, *Ultrason. Sonochem.* **29**, 470 (2016).
[10]. J. Malick, N. Virginie, B. Julien, L.B. Jean, *J. Alloys Compd.* **496**, 306 (2010).
[11]. G.H. An, T.Y. Hwang, Y.H. Choa, S. Kyoosik, *J. Electron. Mater.* **43**, 3574 (2014).
[12]. S.E. Shirsath, S.S. Jadhav, M.L. Mane, S. Li, *Ferrites obtained by sol-gel method. In: Handbook of sol-gel science and technology,* Eds. L. Klein, M. Aparicio, A. Jitianu (Springer, 2016) pp. 1-41.
[13]. B. Hamid, B. Want, *J. Appl. Phys.* **122**, 1 (2016).
[14]. J. Luo, *Mater. Lett.* **80**, 162 (2012).
[15]. H. Khanmohammadi, E.S. Seyyed, *Funct. Mater. Lett.* **4**, 283 (2011).
[16]. M. Effendi, E. Solihah, C. Kurniawan, W.T. Cahyanto, W. Widanarto, *Key Eng. Mater.* **855**, 255 (2020).
[17]. M.A. Almessiere, Y. Slimani, A. Baykal, *Ceram. Int.* **45**, 963 (2019).
[18]. T. Pérez, I. Betancourt, S.P. Sánchez, M.M. García, J.M. Aquino, A.L. Guerrero, *J. Supercond. Nov. Magn.* **24**, 2325 (2011).
[19]. K. Takeyuki, N. Tatsuya, Y. Tohru, N. Makoto, F. Tatsuo, T. Jun, I. Yasunori, *J. Magn. Magn. Mater.* **322**, 2381 (2010).
[20]. P. Kumar, A. Gaur, *Superlattices Microstruct.* **120**, 305 (2018).

[21]. M. Ghimire, D. Kunwar, J. Dahal, D. Neupane, S. Yoon, S. Mishra, *Mater. Sci. Appl.* **11**, 474 (2020).

[22]. Y. Yang, D. Huang, F. Wang, J. Shao, *Chin. J. Phys.* **57**, 250 (2019).

[23]. M. Elansary, M. Belaiche, C. Ahmani, E. Iffer, I. Bsoul, *RSC Adv.* **10**, 25239 (2020).

[24]. M. Changye, M. Zhijun, L. Jun, R. Mingjun, Z. Xin, P. Zhiwei, *J. Rare Earths.* **39**, 1415 (2021).

[25]. A. Hashhash, A. Hassen, W.S. Baleidy, H.S. Refai, *J. Alloys Compd.* **873**, 1 (2021).

[26]. C. Lei, S. Tang, Y. Du, *Ceram. Int.* **42**, 15511 (2016).

[27]. A.Z. Simoes, C. Quinelato, A. Ries, B.D. Stojanovic, E. Longo, J.A. Varela, *Mater. Chem. Phys.* **98**, 481 (2006).

[28]. M. Ferrari, L. Lutterotti, *J. Appl. Phys.* **76**, 7246 (1994).

[29]. X. Obradors, X. Solans, A. Collomb, D. Samaras, J. Rodríguez, M. Pernet, M. Font, *J. Solid State Chem.* **72**, 218 (1988).

[30]. A. Thakur, R.R. Singh, P.B. Barman, *Mater. Chem. Phys.* **141**, 562 (2013).

[31]. Q. Fang, H. Cheng, J. Huang, R. Wang, R. Li, Y. Jiao, *J. Magn. Magn. Mater.* **294**, 281 (2005).

[32]. S. Cotton, *Electronic and magnetic properties of the lanthanides. In: Lanthanide and actinide chemistry*, Ed. S. Cotton (Wiley, 2016) pp. 61-87.

[33]. B. Hamid, B. Want, *Appl. Phys. A* **122**, 148 (2016).

[34]. P. Kumar, S.K. Sharma, M. Knobel, J. Chand, M. Singh, *J. Electroceramics* **27**, 51 (2011).

[35]. N. Rezlescu, C. Doroftei, E. Rezlescu, P.D. Popa, *J. Alloys Compd.* **451**, 492 (2008).

[36]. M.J. Iqbal, S. Farooq, *Mater. Res. Bull.* **46**, 662 (2011).

[37]. M.N. Ashiq, M.J. Iqbal, I.H. Gul, *J. Alloys Compd.* **487**, 341 (2009).

[38]. A. Thakur, R.R. Singh, P.B. Barman, *Mater. Chem. Phys.* **141**, 562 (2013).

[39]. E.C. Stoner, E.P. Wohlfarth, *Philos. Trans. Roy. Soc.* **240**, 599 (1948).

[40]. B.H. Bhat, B. Want, *Appl. Phys.* **122**, 1 (2016).

[41]. M. Naeem, A. Sami, S. Farooq, M. Najam, S. Rehman, *J. Magn. Magn.* **444**, 426 (2017).

[42]. M.M. Rashad, I.A. Ibarhim, *J. Supercond. Nov. Magn.* **26**, 1639 (2013).

[43]. G. Nabiyouni, A. Ahmadi, D. Ghanbari, H. Halakouie, *J. Mater. Sci. Mater.* **27**, 1 (2016).

[44]. J. Lee, E.J. Lee, T.Y. Hwang, J. Kim, Y.H. Choa, *Sci. Rep.* **10**, 1 (2020).

[45]. Q. Li, J. Song, M.S. Múzquiz, F. Besenbacher, M. Christensen, M. Dong, *Sci. Rep.* **6**, 1 (2016).